International Journal of Nanomedicine

Dovepress
open access to scientific and medical research

Open Access Full Text Article

ORIGINAL RESEARCH

In vitro molecular study of wound healing using biosynthesized bacteria nanocellulose/silver nanocomposite assisted by bioinformatics databases

This article was published in the following Dove Press journal:
International Journal of Nanomedicine

Mona Moniri[1,2]
Amin Boroumand Moghaddam[1,2]
Susan Azizi[1]
Raha Abdul Rahim[3]
Saad Wan Zuhainis[4,5]
Mohammad Navaderi[6,7]
Rosfarizan Mohamad[1,5]

[1]Department of Bioprocess Technology, Faculty of Biotechnology and Biomolecular Sciences, Universiti Putra Malaysia, UPM Serdang, Selangor, Malaysia; [2]Young Researcher and Elite Club, Sabzevar Branch, Islamic Azad University, Sabzevar, Iran; [3]Department of Cell and Molecular Biology, Faculty of Biotechnology and Biomolecular Sciences, Universiti Putra Malaysia, UPM Serdang, Selangor, Malaysia; [4]Department of Microbiology, Faculty of Biotechnology and Biomolecular Sciences, Universiti Putra Malaysia, UPM Serdang, Selangor, Malaysia; [5]Institute of Tropical Forestry and Forest Products, Universiti Putra Malaysia, UPM Serdang, Selangor, Malaysia; [6]Young Research and Elite Club, Parand Branch, Islamic Azad University, Parand, Iran; [7]Department of Medical Genetics, National Institute of Genetic Engineering and Biotechnology, Tehran, Iran

Correspondence: Susan Azizi; Rosfarizan Mohamad
Department of Bioprocess Technology, Faculty of Biotechnology and Biomolecular Sciences, Universiti Putra Malaysia, 43400 UPM Serdang, Selangor, Malaysia
Tel +60 17 622 8029; +60 38 946 7518
Fax +60 38 946 8514
Email azisusan@gmail.com; farizan@upm.edu.my

Background: In recent years, bacterial nanocellulose (BNC) based nanocomposites have been developed to promote healing property and antibacterial activity of BNC wound dressing. Molecular study can help to better understanding about interaction of genes and pathways involved in healing progression.

Objectives: The aim of this study was to prepare bacterial nanocellulose/silver (BNC/Ag) nanocomposite films as ecofriendly wound dressing in order to assess their physical, cytotoxicity and antimicrobial properties. The in vitro molecular study was performed to evaluate expression of genes involved in healing of wounds after treatment with BNC/Ag biofilms.

Study design, materials, and methods: Silver nanoparticles were formed by using *Citrullus colocynthis* extract within new isolated bacterial nanocellulose (BNC) RM1. The nanocomposites were characterized using X-ray diffraction, Fourier transform infrared, and field emission scanning electron microscopy. Besides, swelling property and Ag release profile of the nanocomposites were studied. The ability of nanocomposites to promote wound healing of human dermal fibroblast cells in vitro was studied. Bioinformatics databases were used to identify genes with important healing effect. Key genes which interfered with healing were studied by quantitative real time PCR.

Results: Spherical silver nanoparticles with particle size ranging from 20 to 50 nm were synthesized and impregnated within the structure of BNC. The resulting nanocomposites showed significant antibacterial activities with inhibition zones ranging from 7±0.25 to 16.24±0.09 mm against skin pathogenic bacteria. Moreover, it was compatible with human fibroblast cells (HDF) and could promote in vitro wound healing after 48h. Based on bioinformatics databases, the genes of *TGF-β1*, *MMP2*, *MMP9*, *CTNNB1*, *Wnt4*, *hsa-miR-29b-3p* and *hsa-miR-29c-3p* played important role in wound healing. The nanocomposites had an effect in expression of the genes in healing. Thus, the BNC/Ag nanocomposite can be used to heal wound in a short period and simple manner.

Conclusion: This eco-friendly nanocomposite with excellent antibacterial activities and healing property confirming its utility as potential wound dressings.

Keywords: bioinformatics study, wound healing, bacterial nanocellulose, molecular study, gene expression, *Citrullus colocynthis*

Introduction

Bacterial nanocellulose (BNC) is produced by the fermentation of Gram-negative bacterium *Gluconacetobacter xylinus*, which can produce high-aspect ratio nanofibers, with three-dimensional (3D) porous networks.[1,2] It has been utilized in many medical

submit your manuscript | www.dovepress.com
Dovepress
http://dx.doi.org/10.2147/IJN.S164573

and nonmedical applications including use for food industry,[3] acoustic diaphragm, functional paper,[4] drug delivery,[5] tissue engineering,[6] wound dressing, and skin repairs.[7,8]

In the processing of skin tissue healing, the moisture environment provided by the dressing materials has been displayed to help wounds healing and decrease pain of patients. This nanofibrous BC hydrogel is capable of retaining a high quantity of water in itself and provide the needed moisture for healing wounds. It similarly has an adequate compatibility, which decreases the sensitivity and wound pain. Biologic sheet inhibits microbes and pollutants from entering the wound bed owing to the nanofibers and thick structure.[1,9]

Silver has been established to be a favorable candidate for antibacterial activity toward a broad range of pathogenic bacteria.[10] Sliver nanoparticles (Ag-NPs) are extensively used in the pharmaceutical products in the fabrication of creams and ointments to prevent burn- and wound-relevant infections.[11] BNC has no antibacterial activity and it is not able to hinder wound infections. Hence, BNC-based antibacterial composites are usually fabricated. Numerous research groups combined drug,[12] polymers,[13] and nanoparticles[13] in BNC to fabricate wound dressing composites with antibacterial capability, but the result was not so favorable as either they applied toxic materials in synthesis process or few successful results have been reported. In most studies chemical methods have been applied to prepare Ag-NPs, which restrict the medical uses of nanocomposites, due to the toxicity of starting materials.[14] Nowadays, to overcome the complication of toxicity in the production, biomass materials such as plant extracts, microorganism, and enzymes have been well known to have an important role in the nanoparticle synthesis procedure.[15] Bioconstituents of different plant extracts are known as potential synthesizers and stabilizers of metal nanoparticles. In addition, the plant metabolites with pharmaceutical effects have the potential to be introduced on the nanoparticle surfaces during the synthesis procedure, which eventually leads to the occurrence of subsequent different surface effects in their medical applications.[16] Considering the advantages of biologic synthesis of metallic nanoparticles, we developed a green approach to synthesize Ag-NPs with fruit extract of *Citrullus colocynthis* (*C. colocynthis*).

C. colocynthis (Bitter Apple), a member of the *Cucurbitaceae* family, is an important and widely utilized plant in traditional medicine distributed throughout Asia. It has been described to have plentiful important biologic properties, for example antioxidant,[17] anticancer,[18] anti-inflammatory,[19] and antimicrobial[20–22] activities. The fruit contains phytochemicals such as glycosides, flavonoids, alkaloids, carbohydrates, fatty acids, and essential oil,[23] which are capable of reduction and stabilization with biologic activities that motivate our interest to utilize it in the synthesis of Ag-NPs.

Bioinformatics is an interdisciplinary field that aids to simplify scientific investigation of relevant diseases, genes, and pathways based on co-citations. Wound curing is a dynamic process that is controlled by a combination of the molecular regulators. During healing, chemosensory stimulus plays a critical role in directional cell migration. Chemoattractants are small soluble molecules that promote distribution of fibroblasts, T cells, and macrophages throughout the wound site.[24] Key effectors in wound healing process can be identified by bioinformatics databases.

In this study, we have first demonstrated in situ green synthesis of Ag-NPs using *C. colocynths* fruit extract in BNC fibers and characterization of the fabricated BNC/Ag nanocomposites. Secondly, antibacterial activity, cytotoxicity, and healing properties of the prepared BNC/Ag nanocomposites were examined. Through bioinformatics study, the chemo interaction genes that play a critical role in healing process were selected. Finally, pivotal genes that interfered with healing were investigated by quantitative real-time polymerase chain reaction (qRT-PCR).

Materials and methods

Preparation of pure BNC

According to a previous study, the pellicle products of *G. xylinus* (RM1) were obtained from rotten pineapple by fermentation process on modified Hestrin–Schramm medium (pH 5.5) within 24 days at room temperature (30°C) on stirring. Subsequently, the pellicles were rinsed with distilled water and boiled in NaOH (1M) solution for pellicles purification.

Preparation of *C. colocynths* extract

Fresh fruits were dried at room temperature and then milled to smooth powder by a grinder. The powder that passed through an 80-mesh sieve was used for extraction purpose. Briefly, the fine material was extracted with ethanol for 8 hours in a Soxhlet apparatus. The solvent was removed by rotary evaporation.[14] The dried, crude concentrated extract was then stored in a refrigerator (4°C).

Biosynthesis of BNC/Ag nanocomposites

In this study, Ag-NPs were formed into BNC pellicles by a green method to prepare BNC/Ag nanocomposites. At first, silver nitrate ($AgNO_3$) was impregnated into BNC by immersing BNC pellicles (2 g) in different concentrations

of the aqueous $AgNO_3$ (1.0–16.0 wt%) under continuous stirring. After the Ag ions in the suspension were dispersed well, 20 mL of *C. colocynths* fruit extract was poured into the reaction mixture under gentle stirring at 45°C and the reaction was temporarily sustained until the color of the reaction mixture altered from yellow to dark brown, followed by ultrasonication for 30 minutes. For purification of Ag-NPs, the obtained solution was centrifuged at 5,000 rpm for 15 minutes. Then, the supernatant liquid was removed and the samples were washed with distilled water several times and poured into plate dishes and subsequently dried in the freeze drier. The obtained sample films based on the percentage of applied Ag precursors (1.0, 4.0, 8.0, and 16.0 wt%) were called BNC/$Ag_{(1.0\%)}$, BNC/$Ag_{(4.0\%)}$, BNC/$Ag_{(8.0\%)}$, and BNC/$Ag_{(16.0\%)}$.

Characterization of BNC/Ag nanocomposites

The X-ray diffraction (XRD) analysis of the dried original BNC, pure Ag-NPs, and BNC/Ag nanocomposites (1.0%–16.0%) was performed by Philips X'Pert PXRD with Cu-Kα radiation (λ=1.5406 Å), operating at 40 kV in the scan range of 2θ from 2° to 80°. Fourier-transform infrared (FTIR) spectra of nanocomposites were recorded by PerkinElmer 1725X at a frequency range of 4,000–400 cm^{-1}. The morphologic characteristics of specimens were viewed using field emission scanning electron microscopy (FESEM) (JCM-6360LA Philips). UTHSCSA ImageTool software was used to measure the particle size and the size distribution of the Ag-NPs. The size and the particle size distribution of Ag-NPs were estimated by measuring the diameters of about 50 particles selected randomly with the FESEM images of BNC/Ag (1.0–16.0 wt%).

Swelling study of BNC/Ag nanocomposites

The kinetics of swelling was evaluated through periodically assessing weight increase of the films according to the method by Lavorgna et al.[25] The swelling ratio (Q) was evaluated by immersion of 100 mg of BNC/Ag nanocomposites in 0.01 M PBS, pH 7.4, at 37°C. The swollen sample films were taken from the solution at different time periods and excess water was removed from the surface by blotting on wet filter paper and weighted. The Q of bionanocomposites was assessed according to Eq (1):

$$Q = \frac{(w_2 - w_1)}{w_1}$$

where w_1 is the initial weight of the sample and w_2 is the weight of the swollen sample. The equilibrium swelling ratio (Q_{equil}) was measured at the point the BNC/Ag nanocomposites reached a constant weight value. The swelling capacities were computed in triplicate (n=3).

In vitro release assessment of BNC/Ag nanocomposites

The Ag release profile from BNC/Ag nanocomposites was measured by using inductively coupled plasma atomic emission spectrometry (Perkin Elmer 1000, USA). First, the samples were cut to a size of 1×1×0.1 cm^3 and immersed in falcon tubes containing 10 mL of PBS solution (PBS, pH 7.4) at 37°C. The PBS solution was collected at specific time points (6, 12, 24, 48, 72, and 96 hours) and then the same volume of fresh PBS solution was added. The release profile of Ag from BNC nanocomposites was studied using the release kinetics Ritger-Peppas model,[26] a semi empirical power law described by Eq (2)

$$\frac{Ct}{Ceq} = kt^n$$

where Ct and Ceq are the dense concentrations of Ag released from the nanocomposite at a specified time and at equilibrium, respectively, k is a characteristic constant of the hydrogel, and n is the diffusional coefficient used to interpret the release mechanism.

Antibacterial activity

Antibacterial activity of BNC/Ag nanocomposites with different concentrations (1.0, 4.0, 8.0, and 16.0 wt%) was evaluated by the disk diffusion approach against Gram-positive (*Staphylococcus aureus* and *Staphylococcus epidermidis*) and Gram-negative (*Pseudomonas aeruginosa*) bacteria on Muller-Hinton agar. The Ag-NPs-impregnated BNC was cut into a disk shape of 1.5 mm diameter. Afterward, the disk shapes were sterilized by autoclaving for 20 minutes at 121°C, placed on the agar petri dishes, which were already inoculated with 100 µL of photogenic bacteria and inoculated overnight at 37°C. The antibacterial activity of samples was measured by observing the inhibition zone formed surrounding the disks. The inhibition zone was calculated by averaging three independent experiments.

In vitro cytotoxicity assay

A normal cell line (human dermal fibroblast, HDF) was purchased from American Type Culture Collection (Manassas,

VA, USA) and was used to test the in vitro cytotoxicity effect of different concentrations of BNC/Ag nanocomposites (1.0, 4.0, 8.0, and 16.0 wt%) by MTT (3-[4,5-dimethylthiazol-2-yl]-2,5-dephenyl-tetrazolium bromide)[27] approach before performing scratch assay and further analysis. HDF cells were cultured in DMEM supplemented with 5% fetal bovine serum (FBS) and 1% penicillin-streptomycin at a density of 1×10^6 cells/mL in 96-well plates. The cells were maintained at 37°C, in a humidified incubator containing 5% CO_2 for 24 hours. After removing the old medium, the cells were treated with 0, 31.25, 62.5, 125, 250, and 500 µg/mL concentrations of BNC/Ag nanocomposites solution in DMEM and incubated at 37°C for 3 days. Then, MTT solution (20 µL) was added to each well and further incubated for 4 hours at 37°C. The OD was read with enzyme-linked immunosorbent assay at 570 nm. Each concentration of the sample was utilized in triplicate and the cell viability percentage was calculated as follows:

$$\text{Cell viability (\%)} = \frac{(\text{OD of Control} - \text{OD of Samples})}{\text{OD of Control}} \times 100$$

In vitro scratch assay

The spreading and migration capabilities of HDF cells were assessed using a scratch wound assay, which measures the expansion of a cell population on surface.[28,29] According to protocol, HDF cells were cultured into a 24-well plate at a concentration of 3×10^5 cells/mL cultured in a medium containing 5% FBS and the cells let to grow and confluent for 24 hours at 37°C and 5% CO_2. A wound was generated using a sterile (200 µL) pipette tip. Then, the debris cells were removed through washing with PBS. Untreated cells were used as a negative control. Finally, 62.5 µg/mL of BNC/Ag nanocomposites with concentrations of 1.0, 4.0, 8.0, and 16.0 wt% were added and incubated for 24 hours and the pictures of the migration of cells were taken at various time points (0, 24, and 48 hours) with a camera appended to a microscope.

Bioinformatics study

The most effective genes and chemoattractants in wound healing process were identified by literature mining. Afterward, important genes associated with healing process were studied using different databases (DisGeNET [http://www.disgenet.org], Genetics home research [https://ghr.nlm.nih.gov/], UniProtKB [http://www.uniprot.org/help/uniprotkb], and Expression Atlas [https://www.ebi.ac.uk/gxa/home/]). In addition, Cytoscape v 3.4 was used for analyzing mapping network interaction.

qRT-PCR

RNA extraction

According to scratch results, the best concentration of BNC/Ag nanocomposites (8.0 wt%) was selected for gene regulation study. Briefly, total RNA from the treated and untreated HDF cell line using RNeasy Mini kit (Qiagen, Inc., Valencia, CA, USA) was extracted at three different time points (6, 12, and 24 hours). Based on the protocol, the template was used for qRT-PCR to synthesize complimentary DNA from RNA with an RT² First Strand Kit (Qiagen). Then, a pre-mix with 25 µL was provided, containing 12.5 µL of RT² SYBR®Green ROX TM FAST mastermix (Qiagen), 1.2 µL of primers (RT² qPCR Primer Assays, Qiagen), 1 µL of cDNA, and 10.3 µL RNase-free water.

MicroRNA (miRNA) extraction

miRNA (≤200 nucleotides) was extracted from total RNA of HDF cell line using mirVana™ miRNA Isolation Kit (Ambion, Austin, TX, USA). The concentration of RNA was quantified by the absorbance at 260 nm. Poly (A) polymerase (Takara) was used for RNA polyadenylation. According to the manufacturer's instructions the reaction includes the preparation of a mixture of enzyme, enzyme buffer, and the isolated miRNA, and then incubation at 37°C for 1 hour. The Reverse Transcription procedure was performed using a SuperScript III (invitrogen) kit. Table 1 demonstrates that primer pairs of genes, β-*actin*, and *5srRNA* were picked out.

The PCR default conditions were as follows: to activate the enzyme for 5 minutes, the conditions were set to 95°C, and then 40 and 35 cycles for 30 seconds at 95°C (denaturation) were carried out, followed by a 30-second cycle at 60°C (annealing and synthesis) and 30 seconds at 72°C for RNA and miRNA, respectively. Finally, the dissociation curve was built to check and justify the results right after the PCR run. The expression of all genes (*TGF-β1*, *MMP2*, *MMP9*, *Wnt4*, β-*catenin*, *has-miR-29b*, and *hsa-miR-29c*) was compared with the housekeeping genes (β-*actin* and *5srRNA*). Relative gene expression was calculated for each mRNA marker using the $2^{-\Delta\Delta Ct}$ method: $2^{\Delta\Delta Ct} = 2Ct$ (treated cells)−Ct (control cells), where 2 is a derivation of the amplification efficiency doubling the template in each cycle while ascending in strength.

Table 1 Genes used in quantitative real-time polymerase chain reaction

Genes	Forward primer	Reverse primer
TGF-β1	5′-CCCTGGACACCAACTATTGC-3′	5′-CCTACATTTGGAGCCTGGAC-3′
Wnt4	5′-CAGTCGTTTGTGGATGTGCG-3′	5′-GTTTGATGGTGCCACTGAGG-3′
MMP2	5′-CTAGGGCTGGACTCTACATC-3′	5′-GGCCTCCTGATGACAAATGC-3′
MMP9	5′-GAAGATGCTGCTGTTCAGCG-3′	5′-GAGTGAGTTGAACCAGGTGG-3′
CTNNB1	5′-CTTCACATCCTAGCTCGGGA-3′	5′-GCTATTGAAGCTGAGGGAGC-3′
β-actin	5′-GCATCCTCACCCTGAAGTAC-3′	5′-GTACCACTGGCATCGTGATG-3′
5srRNA	5′-CGGCCATACCACCCTGAAC-3′	5′-CCTACAGCACCCGGTATTC-3′
hsa-miR-29b	5′-UAGCACCAUUUGAAAUCAGUGUU-3′	–
hsa-miR-29c	5′-UAGCACCAUUUGAAAUCGGUUA-3′	–

Statistical analysis

Statistical analysis was performed using Graph pad prism software version 7.01 (GraphPad Software Inc., La Jolla, CA, USA). Results were analyzed by one-way analysis of variance. A difference was considered to be significant at $P<0.05$.

Results and discussion

Characterization of BNC/Ag nanocomposites

In this study, Ag-NPs were synthesized using the fruit extract of *C. colocynths* as a reducing agent in BNC hydrogel, a stabilizer for immobilization of the Ag-NPs without using any toxic chemical materials. The synthesis of Ag-NPs was monitored with the color change of reaction suspensions from yellowish to brown after 30 minutes of incubation time. Fruit extract of *C. colocynths* was remarkably effective on the formation of Ag-NPs because of having abundant reducing groups such as hydroxyl (O–H) and carbonyl (C=O) in their structures. BNC was also used as a stabilizer to immobilize NPs because of having plentiful hydroxyl groups and anionic character. The interaction of Ag nanoparticles with the BNC inhibits further nanoparticles combination by stabilizing the particles.

XRD analysis

The XRD patterns for BNC/Ag nanocomposites and pure BNC are exhibited in Figure 1. The two sets of diffraction peaks related to BNC and Ag-NPs have been shown in the XRD patterns of nanocomposites. Two main diffraction peaks showed at 2θ=14.01° and 22.23° are attributed to the BNC. The characteristic peaks of Ag-NPs that are located at 2θ=37.17°, 46.07°, and 64.81° and its corresponding lattice plane value were indexed at (1 1 1, 2 0 0) and (2 2 0) planes of face-centered cubic nature. Because of the comparable typical peaks that can be detected in BNC/Ag nanocomposites, it

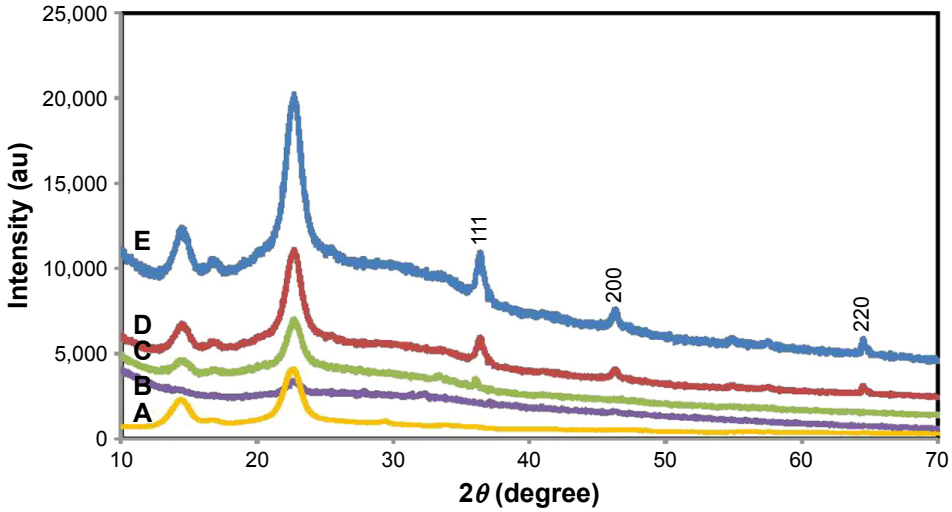

Figure 1 X-ray diffraction patterns of pure BNC (**A**) and BNC/Ag nanocomposites (1.0–16.0 wt%) (**B**–**E**), respectively.
Abbreviation: BNC, bacterial nanocellulose.

can be established that the development of Ag-NPs in BNC did not affect any phase alteration of Ag-NPs. Furthermore, the diffraction peaks of Ag-NPs became steadily strong as the content of Ag was increased, proposing the crystalline structure of the Ag-NPs enhanced.

The average crystal size was estimated using the Debye–Scherrer equation ($D=K\lambda/\beta\cos\theta$), where D is the mean crystal size, K is the Scherrer constant (0.9), λ is the XRD wavelength (0.15418 nm), β is the peak width of half-maximum intensity, and θ is the Bragg diffraction angle. Hence, the average crystal size of the Ag-NPs was measured in the range of 20–50 nm.

FTIR analysis

Figure 2 shows the FTIR spectra of *C. colocynths* fruit extract (**A**), pure BNC (**B**), and BNC/Ag nanocomposites (**C**–**F**). The FTIR spectrum of BNC showed characteristic bands at 3,327, 2,887, 1,677, 1,402, and 1,040 cm^{-1} corresponding to O–H, C–H stretching, O–H bending absorbed water, C–H bending vibration, and C–O–H stretching vibrations, respectively.[30] The FTIR spectrum (Figure 2A) exhibits the structure of *C. colocynths* fruit extract with bands of O–H and C=O at 3,304 and 1,708 cm^{-1}, respectively. After synthesis of Ag-NPs, the position and intensities of peaks were changed in the FTIR spectra of BNC/Ag nanocomposites, indicating the involvement of functional groups of *C. colocynths* fruit extract and BNC in the formation and stabilization of synthesized Ag-NPs. The most important change is related to the presence of a new peak at 1,610 cm^{-1}, which can be attributed to Ag-O band[14] and the peaks at 1,402 and 1,040 cm^{-1} became stronger, which indicates the formation of new bonds between BNC and Ag-NPs and immobilizing of nanoparticles by the BNC matrix.

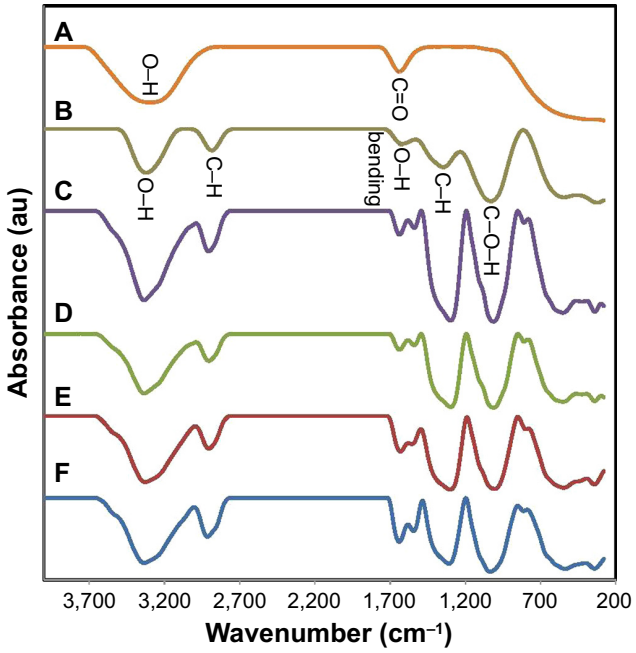

Figure 2 Fourier transform infrared spectra of (**A**) fruit extract, (**B**) pure BNC, and (**C**–**F**) BNC/Ag nanocomposites (16.0–1.0 wt%), respectively.
Abbreviation: BNC, bacterial nanocellulose.

FESEM

FESEM images of pure BNC and BNC containing different concentrations of Ag-NPs are presented in Figure 3A–E. The structure of BNC is 3D nonwoven networks and involves huge number of holes (Figure 3A). Such a 3D network permitted guest molecules to enter throughout its inside space definitely. After BNC being immersed in Ag ions solution, Ag seeds emerged to stick to the surface and interior of BNC fibers (Figure 3B–E), representing the attraction between the nanoparticles and the BNC. As revealed in Figure 3B–E, Ag nanoparticles with spherical shapes were synthesized and immobilized in BNC matrices with the average particle size of 30±5.4, 33±4.3, 35±4.2, and 38±4.2 for BNC/Ag (1.0 to –16.0 wt%) nanocomposites, respectively (inset graphs). The well-distributed Ag-NPs were observed up to 8.0 wt% Ag^{+} loading. Beyond this level most of the nanoparticles formed because of the small dimensions, large specific surface area, and high surface activity were agglomerated[14] (Figure 3E). Thus, the agglomeration of nanoparticles may have an effect on the potential activity and properties of the synthesized Ag-NPs.

Swelling behavior

The swelling capacity is significant for the wound dressing throughout the wound healing process for both the chronic and serious trauma. In this study, the water absorption performance of the BNC and BNC/Ag nanocomposites dry films reflected by the swelling ratio was examined in saline solution.

It was observed from the graph (Figure 4) that the swelling ability increased with time, first quickly and then gradually, reaching an utmost constant swelling. Based on the data, good water-binding capacity with a maximum swelling ratio of 3.19±0.3 for pure BNC and 3.92±0.5, 8.41±0.3, 11.32±0.3, and 10.6±0.2 ($P \leq 0.0001$) for the BNC/Ag nanocomposites (1.0–16.0 wt%) were observed after 120 hours.

The increase in swelling ability was more pronounced in the biocomposite containing 8.0 wt% Ag loading and may be credited to the impregnation of BNC with charged Ag-NPs. The introduction of surface-charged Ag-NPs inside ionic BNC results in an afflux of water to balance the osmotic

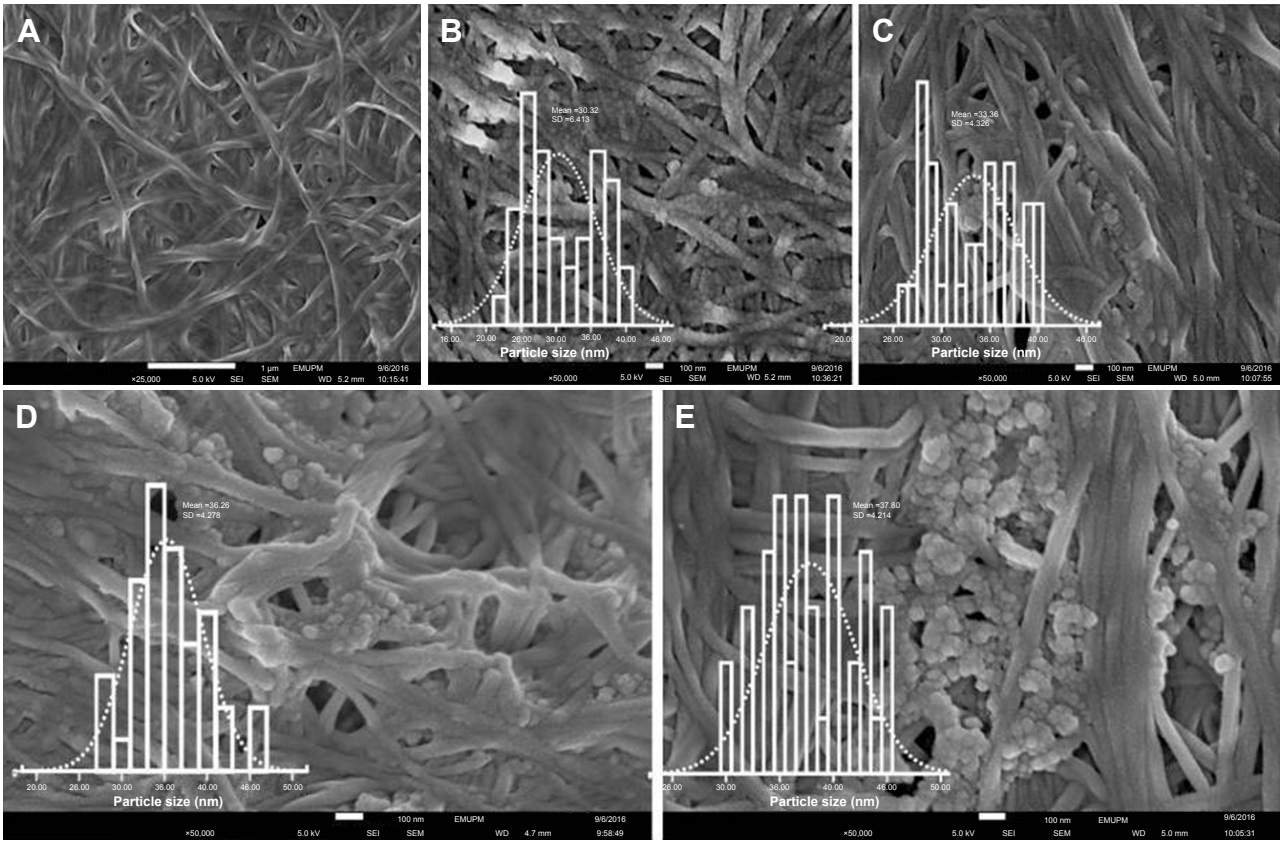

Figure 3 Field emission scanning electron microscopy images of pure (**A**) BNC and (**B**–**E**) BNC/Ag nanocomposites (1.0–16.0 wt%), respectively, and (inset graphs) particle size distribution of Ag-NPs.
Abbreviation: BNC, bacterial nanocellulose.

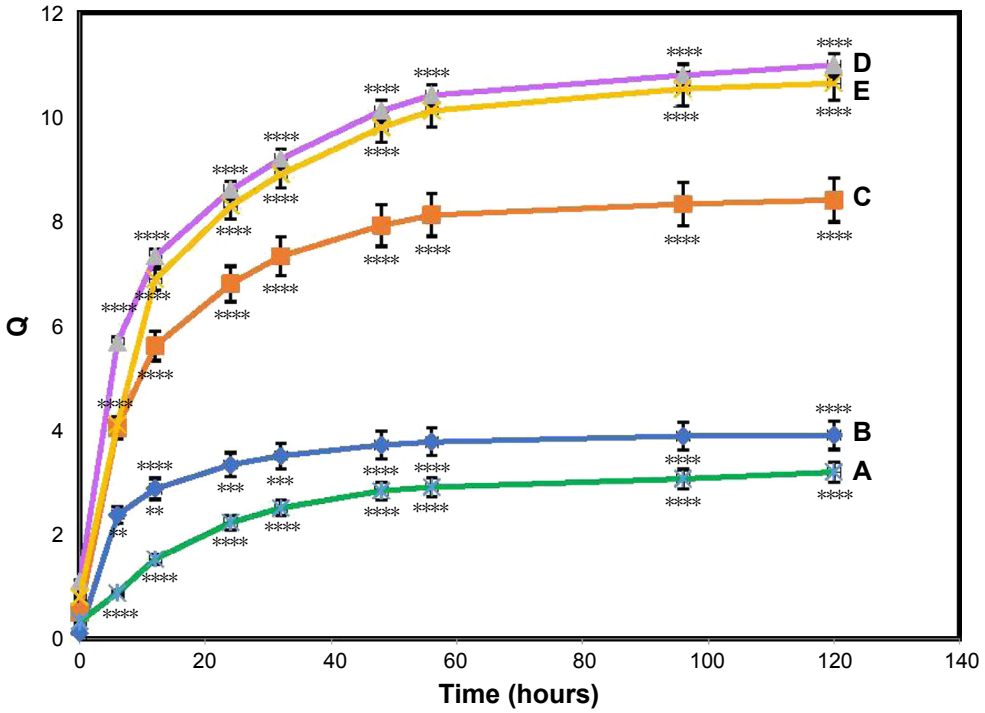

Figure 4 Swelling ratio of pure BNC (**A**) and BNC/Ag nanocomposites (1.0–16.0 wt%) (**B**–**E**), respectively.
Notes: The values represent the mean ± SD (n=3). $^{**}P \leq 0.01$; $^{***}P \leq 0.001$; $^{****}P \leq 0.0001$.
Abbreviation: BNC, bacterial nanocellulose.

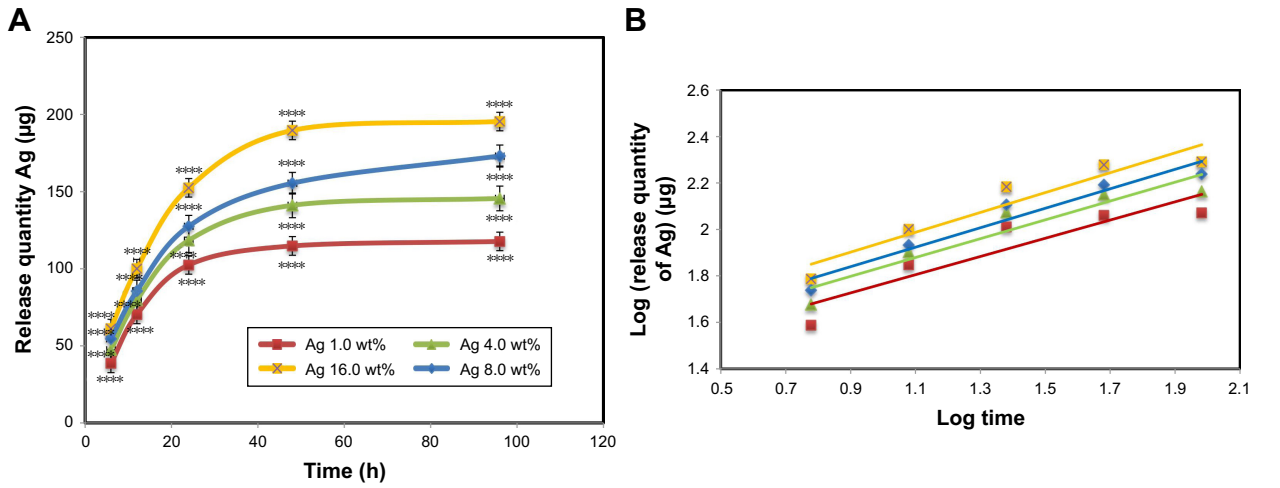

Figure 5 In vitro Ag releasing properties of bacterial nanocellulose/Ag nanocomposites in PBS buffer solution: (**A**) release quantity of Ag in PBS and (**B**) log (release quantity of Ag) vs log (times) curve.
Notes: The values represent the mean ± SD (n=3). ****$P \leq 0.0001$.

pressure buildup, which leads the BNC to swell.[31] More incorporation of Ag-NPs results in an extra strengthening of the polymer network, which will cause the opposite result and limit the swelling of the bionanocomposites.[28]

The equilibrium swelling ratio (Q_{equil}) of the pure BNC was 2.9±0.32. Depending on the content of the Ag-NPs, nanocomposites achieved a higher Q_{equil} than that of the pure BNC.

In vitro Ag releasing properties of BNC/Ag nanocomposites

Ag releasing profile of BNC/Ag nanocomposites in PBS solution is shown in Figure 5A and B. The power law exponent, n, from slopes of the logarithmical curves of Ct/Ceq as a function of time and fitting coefficient (R^2 calculated) is given in Table 2. The results show that n is approximately a similar value for samples, which is indicative of the analogous transport mechanism. When n~0.45, this means that the Ag release mechanism is controlled by Fickian diffusion. The power law exponent of Ag releasing rate of the all tested nanocomposite samples is near to 0.45 with $R^2 \geq 0.836$, which indicates that the Ag release mechanism is controlled by Fickian diffusion.

Table 2 Release quantity and release ratio of Ag from BNC/Ag nanocomposites after 1 and 4 days; slope of fitting and fitting coefficient of log (release quantity of Ag) vs log (times) curve

Sample	Release quantity (µg)		Slope of fitting (n)	Fitting coefficient (R^2)
	1 day	4 days		
$BNC/Ag_{(1.0)}$	38.6±2****	117.6±4	0.391±0.02	0.836
$BNC/Ag_{(4.0)}$	47.4±5****	145.5±3	0.405±0.05	0.884
$BNC/Ag_{(8.0)}$	54.6±3****	173.1±6	0.427±0.03	0.904
$BNC/Ag_{(16.0)}$	85.6±4****	195.4±5	0.418±0.02	0.936

Note: ****$P \leq 0.0001$.
Abbreviation: BNC, bacterial nanocellulose.

It was noticeable that Ag was released from the BNC in the range of 117–195 µg ($P \leq 0.0001$) after 96 hours of release. It is obvious that the release of Ag increased with increasing of the concentration of Ag loading in nanocomposites. The rest of the Ag might have stayed within the BNC because of physical interactions with BNC nanofibers.

Antibacterial activity

The antibacterial performance of BNC/Ag nanocomposites was assessed against Gram-positive (*S. aureus* and *S. epidermidis*) and Gram-negative (*P. aeruginosa*) bacteria by disc diffusion approach. Pure BNC was used as a negative control, and no antibacterial activity was observed. As shown in Table 3, the antibacterial activity of nanocomposites increased with increasing of Ag loading up to 8.0 wt%, and BNC/Ag nanocomposites (8.0 wt%) and (1.0 wt%) had more and less activity, respectively, toward *S. epidermidis*, *S. aureus*, and *P. aeruginosa* with inhibition zones of 14.50±0.09/12±0.1, 16.24±0.09/5.32±0.33, and 15.30±0.38/7±0.25 mm ($P \leq 0.0001$), respectively. Because of their small particle size, Ag-NPs can easily reach the nuclear content of bacteria by disrupting the cell walls of bacteria.[32] In addition, the antibacterial activity of Ag-NPs is also dependent on their shape. On the other hand, the large agglomeration form of BNC/Ag nanocomposites (16.0 wt%) showed a lower antibacterial activity than BNC/Ag nanocomposites (1.0–8.0 wt%), which were less presumable to enter into the cell membrane to damage the inside of bacteria.

Table 3 Inhibition zones (mm) of bacterial nanocellulose/Ag nanocomposites by disk diffusion method against Gram-negative and Gram-positive bacteria

Bacterial strains	Zone of inhibition in mm at different concentrations (wt%)			
	1.0	4.0	8.0	16.0
Pseudomonas aeruginosa	12±0.1****	13.20±0.32****	15.30±0.38****	11±0.1****
Staphylococcus aureus	5.32±0.33****	10.15±0.13****	16.24±0.09****	9±0.2****
Staphylococcus epidermidis	7±0.25****	13.20±0.18****	14.50±0.09****	12±0.3****

Note: ****$P \leq 0.0001$.

Although the mechanism of antibacterial activity of Ag-NPs has not been realized so far,[33] it seems that the accumulation and dissolution of Ag-NPs on the surface of the bacterial membrane causes "pits" to form in the cell membrane (damaged to the cell wall), and the permeability of the membrane changes (progressive release of intracellular factors lipopolysaccharides and membrane proteins).[34] Another reason for antibacterial activity of BNC/Ag nanocomposites is owing to the release of Ag ions (Ag^+) from the BNC/Ag that later penetrate into the bacterial cells and interact by damaging the cell membrane.[33,35] Furthermore, the chemical surface of Ag-NPs plated with biomolecules of *C. colocynths* extract with antibacterial ability can be effectual on the antibacterial activity of Ag-NPs.

Cytotoxicity assay

HDF cells were exposed with varying concentrations of BNC/Ag nanocomposites (1.0–16.0 wt%) before performing a biomedical study. The result of the cytotoxicity showed that BNC/Ag nanocomposites were less toxic to normal HDF cell line after 72 hours of incubation (Figure 6). The viability of cells at the highest concentration (500 µg/mL) of Ag 16.0 wt% was around 60%. The percentage of cells declined with the increase in silver concentration, but it did not affect the cellular activity of HDF cells much even at the highest concentration of 500 µg/mL. Based on the antibacterial and cytotoxicity results, it was found that the BNC/Ag nanocomposites (8.0 wt%) had the best antibacterial activity and least toxicity against cells.

In vitro wound healing assay

The effect of BNC/Ag nanocomposites on HDF cell line migration was determined through scratch assay (Figure 7). The images of the scratch test at 0, 24, and 48 hours after scratching illustrated that the HDF migration into the wound area was accelerated in the presence of BNC/Ag

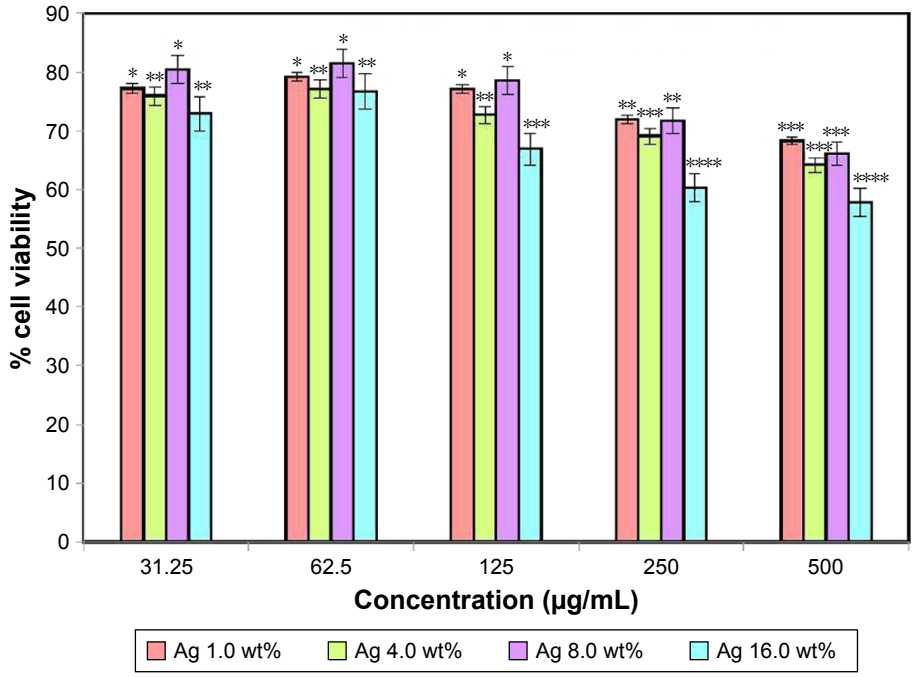

Figure 6 Effect of bacterial nanocellulose/Ag nanocomposites on the viability of human dermal fibroblast cells.
Notes: The values represent the mean ± SD (n=3). *$P \leq 0.05$; **$P \leq 0.01$; ***$P \leq 0.001$; ****$P \leq 0.0001$.

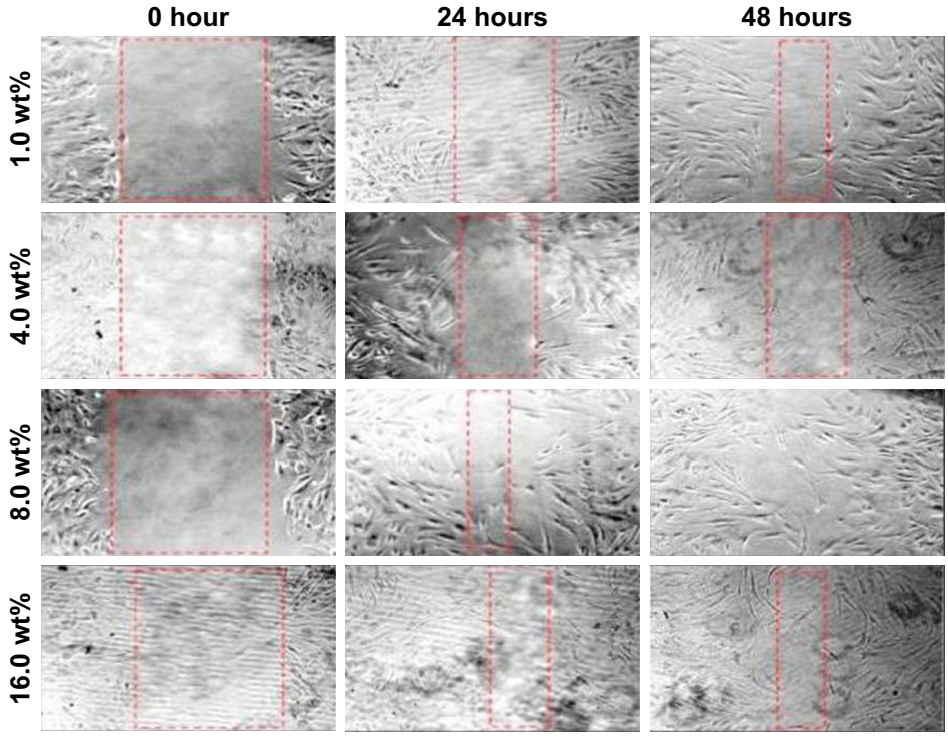

Figure 7 In vitro scratch assay.
Note: Human dermal fibroblast cells were injured and cell migration assay with and without treatment was performed at different time duration (0, 24, and 48 hours) and different concentrations of bacterial nanocellulose/Ag nanocomposites.

nanocomposites. After 48 hours, the scratch was closed with BNC/Ag nanocomposites (8.0 wt%); in contrast, negative control (untreated cells) required more time to get closure. According to the best results of MTT, antibacterial activity, and scratch assay, the BNC/Ag nanocomposites (8.0 wt%) were chosen for gene regulation study.

Bioinformatics study

According to literatures, in PubMed databases, the most effective genes and miRNAs (transforming growth factor β1 [*TGF-β1*], *MMP2*, *MMP9*, *CTNNB1*, *Wnt4*, *has-miR-29-3p*, and *has-miR-29c-3p*) in healing of wounds were documented. As the chemotaxis migration of cells toward the injure site play an important role, we attempted to study the correlation between genes and chemoattractant regulators in wound healing process.

The networks interactions of genes, miRNAs, and chemotaxis regulators in wound healing were drawn by using Cytoscape v 3.4 (Figure S1). Consequently, *TGF-β*, *CTNNB1*, *MMP2*, *MMP9*, and *WNT4* genes possess an impact potential to control the wound healing process with the combination of chemoattractants like *EGF*, *FGF2*, *FGF7*, *VEGF*, *GMCSF*, *PDGFa*, *CTGF*, *CCL2*, *CCL3*, *CXCL1*, and *CXCL8* (Figure S2).

miRNAs are important regulators of wound healing gene expression. The network interaction between miRNA gene including 93 nodes (miRNAs and miRNA targets) and 183 directed edges is given in Figure S3. Similarly, the hsa-miR-29b-3p and has-miR-29c-3p are the most potential regulators of the mentioned genes in wound healing process. Figure 8 shows the direct interactions between these miRNAs and their target genes. These genes and miRNAs were selected for molecular study (qRT-PCR).

Gene expression study by qRT-PCR

In this research, the effect of BNC/Ag nanocomposites (8.0 wt%) on healing genes (*TGF-β1*, *MMP2*, *MMP9*, *CTNNB1*, *Wnt4*, *has-miR-29-3p*, and *has-miR-29c-3p*) in the HDF cell line at three different time periods (6, 12, and 24 hours) was evaluated by qRT-PCR. The *TGF-β* is involved in a number of processes in the wound healing, which include inflammation, stimulating angiogenesis, fibroblast proliferation, collagen synthesis, and deposition and remodeling of the new extracellular matrix.[36,37] It is interesting to note that the chronic, nonhealing wounds often show a loss of *TGF-β1* signaling.[38,39] Based on the *TGF-β1* results, after treatment with BNC/Ag nanocomposites for various time durations, its expression was upregulated from 4.8- to 11-fold at 6 and 24 hours, respectively ($P<0.0001$).

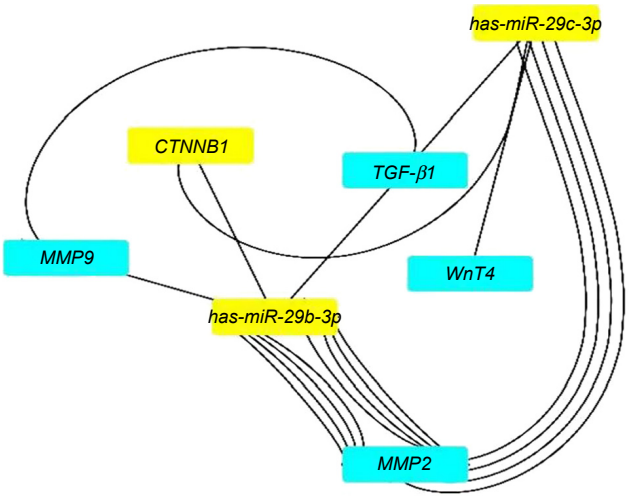

Figure 8 The network interaction analysis between *has-miR-29b-3p* and *has-miR-29c-3p* with their targets.
Note: *has-miR-29b-3p* and *has-miR-29c-3p* have strong interactions with *TGF-β1*, *MMP2*, *MMP9*, *CTNNB1*, and *Wnt4* genes.

The qRT-PCR approach created by Tarnuzzer et al in 1996[40] was utilized to detect the expression of mRNA for *TGF-β1* in acute wounds. They showed that the expression of *TGF-β1* was grown up during healing of cutaneous wounds.[40] In another research in 2001,[41] it was showed that once an ulcer entered a healing phase expression of *TGF-β1*, its receptors were upregulated and at this stage exogenous addition of growth factors could be more effective. This could be of particular importance in the clinical trialing of growth factors for their effects on impaired wound healing.

In the normal wound healing, matrix-metalloproteinase (*MMP*) seems to be involved in various processes. In the first phase of wound repair, MMPs participate in the removal of devitalized tissue. During the repair phase, *MMP* activities are necessary for angiogenesis, contraction of wound matrix, migration of fibroblasts, and for keratinocyte migration and epithelialization. During the final phase of wound healing, *MMPs* participate in the remodeling of newly synthesized connective tissue. In summary, spatially and temporally controlled expression of several distinct *MMPs* is necessary for normal wound healing and tissue repair.[42–46]

MMP2 (gelatinize A) and *MMP9* (gelatinize B) have been widely studied in the cell migration and re-epithelialization, but this study still remains open on how these two proteinases activity *MMP2* is involved during angiogenesis[47] and for the generation of matrix fragments that act as a scaffold for cell migration and a chemotactic signal.[48] In addition, *MMP9* (gelatinase B) promotes migration of a range of epithelial cell types, and it helps in the wound closure.[49,50]

The expression of *MMP2* after treatment with BNC/Ag nanocomposites was upregulated at different durations (6, 12, and 24 hours) of treatment by around 3.1-, 7-, and 9.7-fold respectively; in other words, the expression of *MMP2* was tripled by increasing the incubation time and the level of expression increased significantly. Figure 9 shows that the expression of *MMP9* gene was upregulated from 3.7 to 6.9 at 6–12 hours ($P \leq 0.0001$).

Wnt/β-catenin signaling plays an essential role in the skin development and wound healing.[51,52] *Wnt4* is expressed in the epidermis of both embryonic and adult mouse skin.[53] We hypothesized that BNC/Ag nanocomposites might affect *wnt4* and *CTNNB1* and thus lead to accelerated healing. According to the qRT-PCR result, the expression of the *wnt4* gene in the treated BNC/Ag nanocomposites was upregulated by 5.2-, 8.5-, and 11.4-fold at 6, 12, and 24 hours ($P \leq 0.0001$). The ratio of *CTNNB1* increased from 5.2- to 8.9-fold at 6 and 12 hours, and the mRNA expression after 24 hours grew dramatically as compared to the control.

miRNAs are a novel class of endogenous, small, non-coding RNAs that control gene expression by binding to their target mRNAs for degradation and/or translational repression. *MiR-29* is a typical multifunctional miRNA that is involved in regulating the epithelial–mesenchymal transition, cellular differentiation, extracellular matrix remodeling, and angiogenesis.[54,55] Guo et al illustrated that *miR-29b* was downregulated in thermal injury tissue and *miR-29b* treatment could promote wound healing, inhibit scar formation, and alleviate histopathologic morphologic alteration in scald tissues. Additionally, *miR-29b* treatment suppressed collagen deposition and fibrotic gene expression in scar tissues.[56]

Data analysis of the relative gene expression illustrated that the expression of *has-mir-29b* of HDF cells treated at 6, 12, and 24 hours with nanocomposites was noticeably downregulated by −5.4-, −7.1-, and −10.15-fold, respectively. BNC/Ag nanocomposites had a significant effect on the expression of *has-mir-29c* in HDF cells, because it decreased the level of *has-mir-29c* at 6, 12, and 24 hours −4.7-, −8.3-, and −10.8-fold, respectively. In other words, the ratio of *has-mir-29c* was approximately doubled from 4.7 to 8.3 at 6 and 12 hours ($P < 0.0001$).

Conclusion

This study revealed that the BNC-based Ag nanocomposites were successfully prepared and they showed good antibacterial efficiency and healing properties. The BNC/Ag nanocomposites of concentration 8.0 wt% with good healing property were remarkably effective on *S. aureus*.

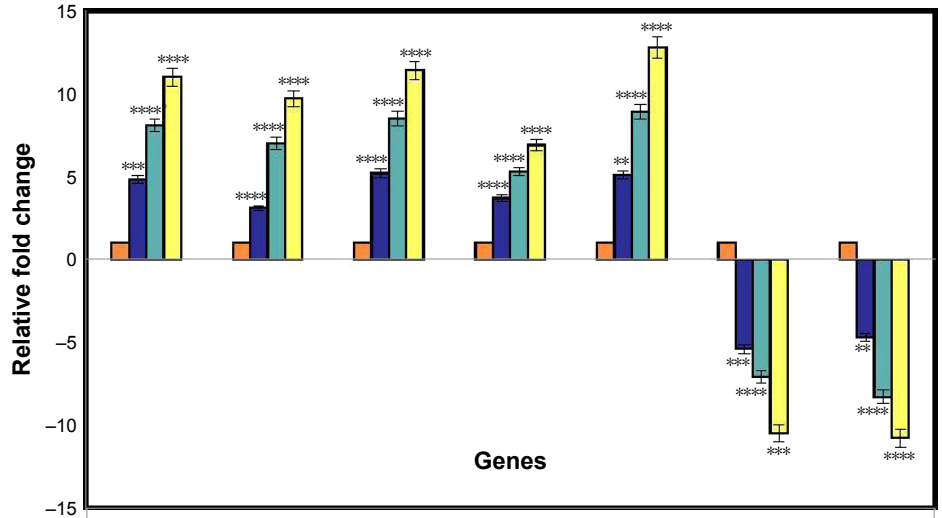

	TGF-β1	MMP2	Wnt4	MMP9	CTNNB1	miR-29b	miR-29c
Control	1	1	1	1	1	1	1
6 hours	4.8	3.1	5.2	3.7	5.1	–5.4	–4.7
12 hours	8.1	7	8.5	5.3	8.9	–7.1	–8.3
24 hours	11	9.7	11.4	6.9	12.8	–10.5	–10.8

Figure 9 Gene expression analysis.
Notes: The graph shows relative fold change for the genes. The values represent the mean ± SD (n=3). **$P \leq 0.01$; ***$P \leq 0.001$; ****$P \leq 0.0001$.

Bioinformatics study showed that *TGF-β1*, *MMP2*, *MMP9*, *CTNNB1*, *Wnt4*, *has-miR-29-3p*, and *has-miR-29c-3p* had strong interaction with each other to promote healing process. The BNC/Ag nanocomposites could increase the expression level of genes (*TGF-β1*, *MMP2*, *MMP9*, *CTNNB1*, and *Wnt4*) and the expression of miRNA (*has-miR-29-3p* and *has-miR-29c-3p*) was downregulated in varying time periods. It was hypothesized that the BNC/Ag nanocomposites might also be tailored for preparing nanomedicines and targeted wound dressing in future.

Our favorable results suggest that the biosynthesized BNC/Ag nanocomposites could be a promising candidate for development of future wound dressings. The nature of biosynthesis and the therapeutic potential of BNC/Ag nanocomposites could pave the way for further research on design of green synthesized wound dressings, to deal with the treatment of infections and healing. Further studies are needed to fully characterize the mechanisms involved with the antimicrobial and healing effects of these nanocomposites.

Acknowledgments

The authors are grateful to the Department of Bioprocess Technology, Faculty of Biotechnology and Biomolecular Sciences, the Institute of Bioscience, Universiti Putra Malaysia and Putra-IPS Grant (Vote Number: 9506000) for the laboratory facilities and funding.

Author contributions

Mona Moniri has performed experiments and written the manuscript. Amin Boroumand Moghaddam has contributed to writing the manuscript. Rosfarizan Mohamad and Susan Azizi have supervised this research and edited the manuscript. Raha Abdul Rahim and Wan Zuhainis Saad have supervised the research. Mohammad Navaderi has analyzed the Bioinformatics data. All authors contributed toward data analysis, drafting and revising the paper and agree to be accountable for all aspects of the work.

Disclosure

The authors report no conflicts of interest in this work.

References

1. Huang Y, Zhu C, Yang J, Nie Y, Chen C, Sun D. Recent advances in bacterial cellulose. *Cellulose*. 2014;21(1):1–30.
2. Wu ZY, Liang HW, Chen LF, Hu BC, Yu SH. Bacterial cellulose: a robust platform for design of three dimensional carbon-based functional nanomaterials. *Acc Chem Res*. 2016;49(1):96–105.
3. Shi Z, Zhang Y, Phillips GO, Yang G. Utilization of bacterial cellulose in food. *Food Hydrocoll*. 2014;35:539–545.
4. Basta AH, El-Saied H. Performance of improved bacterial cellulose application in the production of functional paper. *J Appl Microbiol*. 2009;107(6):2098–2107.
5. Abeer MM, Mohd Amin MC, Martin C, Amin M, Iqbal MC. A review of bacterial cellulose-based drug delivery systems: their biochemistry, current approaches and future prospects. *J Pharm Pharmacol*. 2014; 66(8):1047–1061.

6. Andersson J, Stenhamre H, Bäckdahl H, Gatenholm P. Behavior of human chondrocytes in engineered porous bacterial cellulose scaffolds. *J Biomed Mater Res A*. 2010;94(4):1124–1132.
7. Zhong SP, Zhang YZ, Lim CT. Tissue scaffolds for skin wound healing and dermal reconstruction. *Wiley Interdiscip Rev Nanomed Nanobiotechnol*. 2010;2(5):510–525.
8. Boateng JS, Matthews KH, Stevens HN, Eccleston GM. Wound healing dressings and drug delivery systems: a review. *J Pharm Sci*. 2008;97(8):2892–2923.
9. Lin S-P, Calvar IL, Catchmark JM, Liu J-R, Demirci A, Cheng K-C. Biosynthesis, production and applications of bacterial cellulose. *Cellulose*. 2013;20(5):2191–2219.
10. Sharma VK, Yngard RA, Lin Y. Silver nanoparticles: green synthesis and their antimicrobial activities. *Adv Colloid Interface Sci*. 2009;145(1–2):83–96.
11. Satyavani K, Ramanathan T, Gurudeeban S. Plant mediated synthesis of biomedical silver nanoparticles by using leaf extract of Citrullus colocynthis. *Res J Nanosci Nanotechnol*. 2011;1(2):95–101.
12. Shao W, Wang S, Wu J, Huang M, Liu H, Min H. Synthesis and antimicrobial activity of copper nanoparticle loaded regenerated bacterial cellulose membranes. *RSC Adv*. 2016;6(70):65879–65884.
13. Wu L, Zhou H, Sun HJ, et al. Thermoresponsive bacterial cellulose whisker/poly(NIPAM-co-BMA) nanogel complexes: synthesis, characterization, and biological evaluation. *Biomacromolecules*. 2013;14(4):1078–1084.
14. Azizi S, Mohamad R, Abdul Rahim R, et al. Hydrogel beads bionanocomposite based on Kappa-Carrageenan and green synthesized silver nanoparticles for biomedical applications. *Int J Biol Macromol*. 2017;104(Pt A):423–431.
15. Ahmed S, Ahmad M, Swami BL, Ikram S. A review on plants extract mediated synthesis of silver nanoparticles for antimicrobial applications: a green expertise. *J Adv Res*. 2016;7(1):17–28.
16. Azizi S, Mohamad R, Bahadoran A, et al. Effect of annealing temperature on antimicrobial and structural properties of bio-synthesized zinc oxide nanoparticles using flower extract of Anchusa italica. *J Photochem Photobiol B*. 2016;161:441–449.
17. Kumar S, Kumar D, Manjusha, Saroha K, Singh N, Vashishta B. Antioxidant and free radical scavenging potential of Citrullus colocynthis (L.) Schrad. methanolic fruit extract. *Acta Pharm*. 2008;58(2):215–220.
18. Chen JC, Chiu MH, Nie RL, Cordell GA, Qiu SX. Cucurbitacins and cucurbitane glycosides: structures and biological activities. *Nat Prod Rep*. 2005;22(3):386–399.
19. Graham DY, Agrawal NM, Roth SH. Prevention of NSAID-induced gastric ulcer with misoprostol: multicentre, double-blind, placebo-controlled trial. *Lancet*. 1988;2(8623):1277–1280.
20. Mohammad D, Al-Khateeb M, Riyadh E, Al-Hashem F, Nabil B, Mohammad K. In vivo, acute, normo-hypoglycemic, antihyperglycemic, insulinotropic actions of orally administered ethanol extract of Citrullus colocynthis (L.) Schrab pulp. *Am J Biochem Biotechnol*. 2009;5(3):119–126.
21. Memon U, Brohi AH, Ahmed SW, Azhar I, Bano H. Antibacterial screening of Citrullus colocynthis. *Pak J Pharm Sci*. 2003;16(1):1–6.
22. Najafi S, Sanadgol N, Nejad BS, Beiragi MA, Sanadgol E. Phytochemical screening and antibacterial activity of Citrullus colocynthis (Linn.) Schrad against Staphylococcus aureus. *J Med Plants Res*. 2010;4(22):2321–2325.
23. Salama HMH. Alkaloids and flavonoids from the air dried aerial parts of Citrullus colocynthis. *J Med Plants Res*. 2012;6(38):5150–5155.
24. Janetopoulos C, Firtel RA. Directional sensing during chemotaxis. *FEBS Lett*. 2008;582(14):2075–2085.
25. Lavorgna M, Piscitelli F, Mangiacapra P, Buonocore GG. Study of the combined effect of both clay and glycerol plasticizer on the properties of chitosan films. *Carbohydr Polym*. 2010;82(2):291–298.
26. Ritger PL, Peppas NA. A simple equation for description of solute release I. Fickian and non-fickian release from non-swellable devices in the form of slabs, spheres, cylinders or discs. *J Control Release*. 1987;5(1):23–36.
27. Mosmann T. Rapid colorimetric assay for cellular growth and survival: application to proliferation and cytotoxicity assays. *J Immunol Methods*. 1983;65(1–2):55–63.
28. Muhammad AA, Pauzi NA, Arulselvan P, Abas F, Fakurazi S. In vitro wound healing potential and identification of bioactive compounds from Moringa oleifera Lam. *Biomed Res Int*. 2013;2013(1):1–10.
29. Liang CC, Park AY, Guan JL. In vitro scratch assay: a convenient and inexpensive method for analysis of cell migration in vitro. *Nat Protoc*. 2007;2(2):329–333.
30. Azizi S, Ahmad M, Mahdavi M, Abdolmohammadi S. Preparation, characterization, and antimicrobial activities of ZnO nanoparticles/cellulose nanocrystal nanocomposites. *Bioresources*. 2013;8(2):1841–1851.
31. Salgueiro AM, Daniel-da-Silva AL, Fateixa S, Trindade T. κ-Carrageenan hydrogel nanocomposites with release behavior mediated by morphological distinct Au nanofillers. *Carbohydr Polym*. 2013;91(1):100–109.
32. Bin Ahmad M, Lim JJ, Shameli K, Ibrahim NA, Tay MY, Chieng BW. Antibacterial activity of silver bionanocomposites synthesized by chemical reduction route. *Chem Cent J*. 2012;6(1):101.
33. Maiti S, Krishnan D, Barman G, Ghosh SK, Laha JK. Antimicrobial activities of silver nanoparticles synthesized from Lycopersicon esculentum extract. *J Anal Sci Technol*. 2014;5(1):40.
34. Amro NA, Kotra LP, Wadu-Mesthrige K, Bulychev A, Mobashery S, Liu G-Yu. High-resolution atomic force microscopy studies of the *Escherichia coli* outer membrane: structural basis for permeability. *Langmuir*. 2000;16(6):2789–2796.
35. Hsueh YH, Lin KS, Ke WJ, et al. The antimicrobial properties of silver nanoparticles in Bacillus subtilis are mediated by released Ag^+ ions. *PLoS One*. 2015;10(12):e0144306.
36. Roberts AB, Sporn MB, Assoian RK, et al. Transforming growth factor type beta: rapid induction of fibrosis and angiogenesis in vivo and stimulation of collagen formation in vitro. *Proc Natl Acad Sci U S A*. 1986;83(12):4167–4171.
37. Nall AV, Brownlee RE, Colvin CP, et al. Transforming growth factor beta 1 improves wound healing and random flap survival in normal and irradiated rats. *Arch Otolaryngol Head Neck Surg*. 1996;122(2):171–177.
38. Pastar I, Stojadinovic O, Krzyzanowska A, et al. Attenuation of the transforming growth factor beta-signaling pathway in chronic venous ulcers. *Mol Med*. 2010;16(3–4):1.
39. Kim BC, Kim HT, Park SH, et al. Fibroblasts from chronic wounds show altered TGF-beta-signaling and decreased TGF-beta Type II receptor expression. *J Cell Physiol*. 2003;195(3):331–336.
40. Tarnuzzer RW, Macauley SP, Farmerie WG, et al. Competitive RNA templates for detection and quantitation of growth factors, cytokines, extracellular matrix components and matrix metalloproteinases by RT-PCR. *Biotechniques*. 1996;20(4):670–674.
41. Cowin AJ, Hatzirodos N, Holding CA, et al. Effect of healing on the expression of transforming growth factor beta(s) and their receptors in chronic venous leg ulcers. *J Invest Dermatol*. 2001;117(5):1282–1289.
42. Moses MA, Marikovsky M, Harper JW, et al. Temporal study of the activity of matrix metalloproteinases and their endogenous inhibitors during wound healing. *J Cell Biochem*. 1996;60(3):379–386.
43. Nwomeh BC, Liang HX, Diegelmann RF, Cohen IK, Yager DR. Dynamics of the matrix metalloproteinases MMP-1 and MMP-8 in acute open human dermal wounds. *Wound Repair Regen*. 1998;6(2):127–134.
44. Saarialho-Kere UK, Kovacs SO, Pentland AP, Olerud JE, Welgus HG, Parks WC. Cell-matrix interactions modulate interstitial collagenase expression by human keratinocytes actively involved in wound healing. *J Clin Invest*. 1993;92(6):2858–2866.
45. Soo C, Shaw WW, Zhang X, Longaker MT, Howard EW, Ting K. Differential expression of matrix metalloproteinases and their tissue-derived inhibitors in cutaneous wound repair. *Plast Reconstr Surg*. 2000;105(2):638–647.
46. Young PK, Grinnell F. Metalloproteinase activation cascade after burn injury: a longitudinal analysis of the human wound environment. *J Invest Dermatol*. 1994;103(5):660–664.

47. Itoh T, Tanioka M, Yoshida H, Yoshioka T, Nishimoto H, Itohara S. Reduced angiogenesis and tumor progression in gelatinase A-deficient mice. *Cancer Res*. 1998;58(5):1048–1051.
48. Clark RAF. Wound repair overview and general considerations. *Mol Cell Biol Wound Repair*. 1997;(2):3–33.
49. Mccawley LJ, O'Brien P, Hudson LG. Epidermal growth factor (EGF)- and scatter factor/hepatocyte growth factor (SF/HGF)-mediated keratinocyte migration is coincident with induction of matrix metalloproteinase (MMP)-9. *J Cell Physiol*. 1998;176(2):255–265.
50. Bove PF, Wesley UV, Greul AK, Hristova M, Dostmann WR, van der Vliet A. Nitric oxide promotes airway epithelial wound repair through enhanced activation of MMP-9. *Am J Respir Cell Mol Biol*. 2007;36(2):138–146.
51. Bielefeld KA, Amini-Nik S, Alman BA. Cutaneous wound healing: recruiting developmental pathways for regeneration. *Cell Mol Life Sci*. 2013;70(12):2059–2081.
52. Andl T, Reddy ST, Gaddapara T, Millar SE. WNT signals are required for the initiation of hair follicle development. *Dev Cell*. 2002;2(5):643–653.
53. Reddy S, Andl T, Bagasra A, et al. Characterization of Wnt gene expression in developing and postnatal hair follicles and identification of Wnt5a as a target of Sonic hedgehog in hair follicle morphogenesis. *Mech Dev*. 2001;107(1–2):69–82.
54. Kriegel AJ, Liu Y, Fang Y, Ding X, Liang M. The miR-29 family: genomics, cell biology, and relevance to renal and cardiovascular injury. *Physiol Genomics*. 2012;44(4):237–244.
55. Kogure T, Costinean S, Yan I, Braconi C, Croce C, Patel T. Hepatic miR-29ab1 expression modulates chronic hepatic injury. *J Cell Mol Med*. 2012;16(11):2647–2654.
56. Guo J, Lin Q, Shao Y, Rong L, Zhang D. miR-29b promotes skin wound healing and reduces excessive scar formation by inhibition of the TGF-β1/Smad/CTGF signaling pathway. *Can J Physiol Pharmacol*. 2017;95(4):437–442.

Supplementary materials

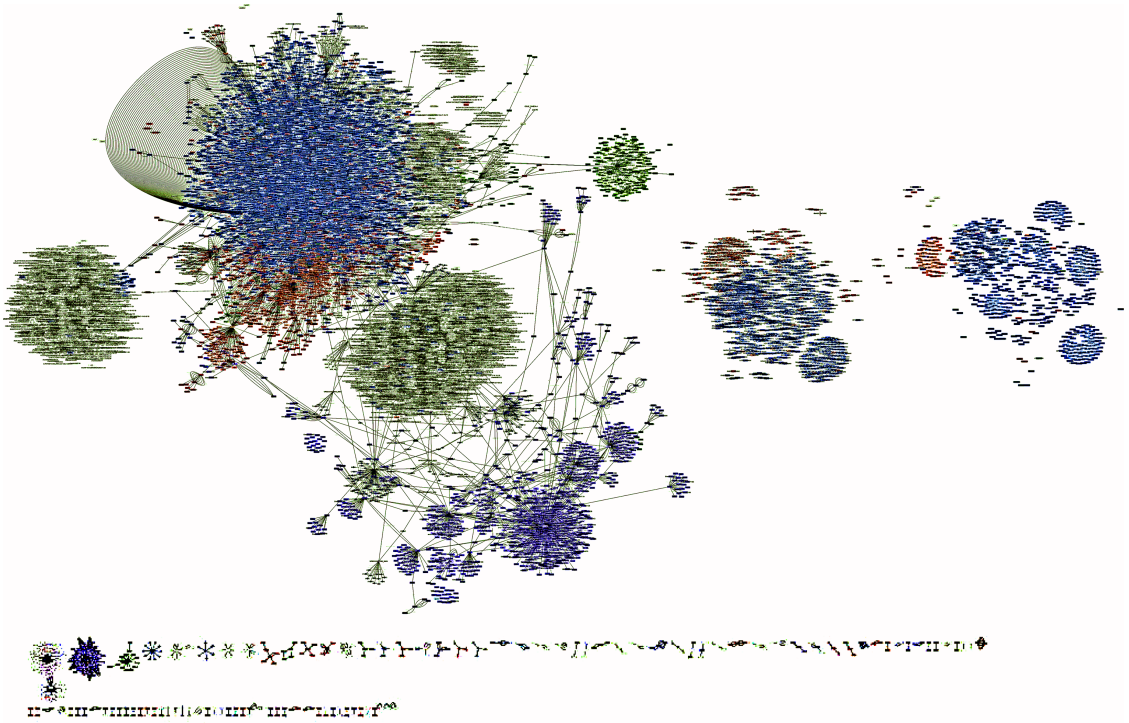

Figure S1 The effect of genes and miRNAs in wound healing process.
Notes: The gene–gene and gene–miRNAs network interaction that included 19,177 nodes and 54,573 edges. The network was mapped through Cytoscape v3.4.

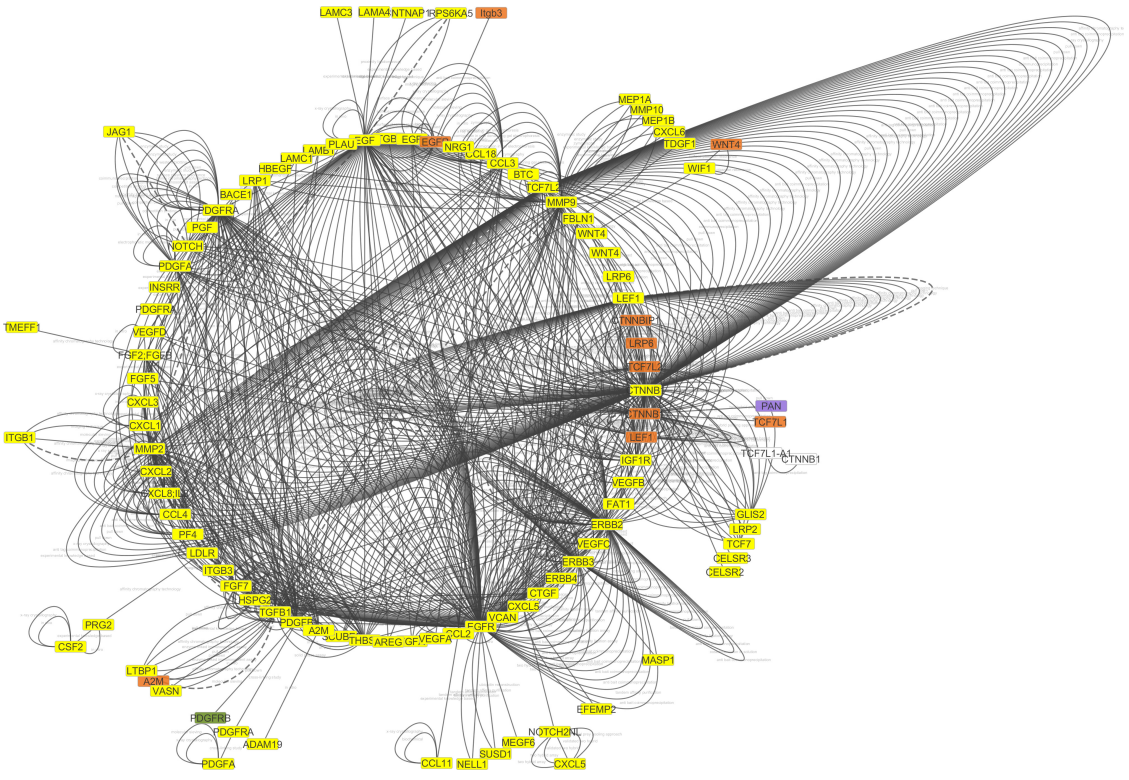

Figure S2 The interaction between genes and chemoattractions in wound healing process.

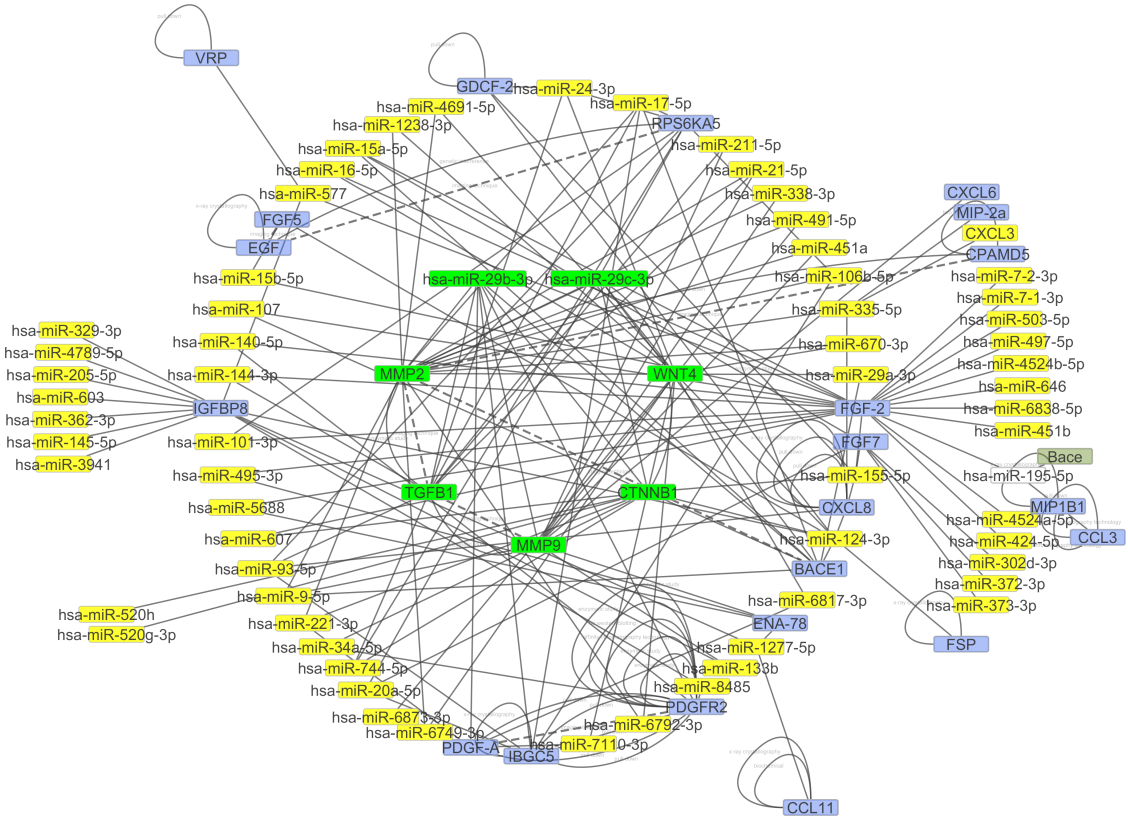

Figure S3 The interaction between gene and miRNAs. The white nodes are miRNAs and the blue ones are genes.